5090 *Biochemistry* **2009,** *48,* 5090–5095
DOI: 10.1021/bi900435m

BIOCHEMISTRY
including biophysical chemistry & molecular biology
Article

PX- and FYVE-Mediated Interactions with Membranes: Simulation Studies[†]

Emi Psachoulia and Mark S. P. Sansom*

Department of Biochemistry, University of Oxford, Oxford OX1 3QU, U.K.

Received March 13, 2009; Revised Manuscript Received May 1, 2009

ABSTRACT: Molecular dynamics simulations have been used to explore the interactions of two PI(3)P-binding domains with their PI ligands and with a phospholipid bilayer. Three simulations each of the EEA1-FYVE domain and the $p40^{phox}$-PX domain have been compared: with the protein in an apo state, with a bound Ins $(1,3)P_2$ molecule, and bound to a PI(3)P molecule embedded in a lipid bilayer. Two main questions were addressed in analysis of the simulations: (i) the location of these domains relative to the lipid bilayer and (ii) their interactions with the lipids, both specific interactions via bound PI(3)P and nonspecific interactions with bilayer phospholipids. Both domains underwent a decrease in dynamic flexibility on binding to the ligand and to the membrane, this being more pronounced for the FYVE domain. Compared to their starting locations [docked to a membrane-inserted PI(3)P molecule], each of the domains penetrated more deeply into the lipid bilayer. For FYVE, nonspecific protein−lipid interactions were formed mainly by the N-terminal hydrophobic region of the protein. For PX, both the α1−α2 and the β1−β2 regions penetrated the bilayer. There appeared to be more marked dynamic fluctuations in hydrogen bonds between basic side chains and PI(3)P for FYVE than for PX, but for both domains, such interactions were maintained throughout the simulations. The simulations agree well with available biophysical data, suggesting this computational method may be used to predict protein−bilayer interactions for other PI-binding proteins.

Phosphosinositides (PIs)[1] play key roles in the control of many processes at cell membranes, e.g., as signal mediators at the cell surface or as regulators of membrane trafficking (*1*, *2*). Of the PIs, PI(3)P is produced in early endosomes and is involved in endosomal membrane trafficking. It binds with high affinity and specificity to two distinct protein domains: the FYVE domain and the Phox homology (PX) domain (*3*).

FYVE domains contain 60−70 amino acids and are double zinc fingers, with each of the two Zn^{2+} ions coordinated by four cysteines (Figure 1). The FYVE domain structure of the early endosome autoantigen (EEA1) (*4*, *5*) consists of two small double-stranded β-sheets and a C-terminal α-helix. Strand β1 contains a conserved basic sequence motif, (R/K)(R/K)HHCR, which is important for PI(3)P binding. The 1-phosphate (P1) of PI(3)P interacts with the first arginine (R1370) of this motif, whereas the 3-phosphate (P3) interacts with the small positively charged pocket created by the HHCR residues as well as a conserved arginine (R1400) in the RVC motif within strand β4 (*4*, *6*). The exact mechanism of membrane binding by FYVE domains has not yet reached consensus, and several possible models have been proposed (*4*−*7*). The membrane binding mechanism is thought to include an initial adsorption of the domain on the membrane by nonspecific interactions (*1*, *7*−*9*), followed by specific ligand binding to PI(3)P, and subsequent interfacial penetration (*8*) of an N-terminal hydrophobic loop located near P1. There may also be protein dimerization (*4*, *10*).

The Phox homology (PX) domain is an ∼130-amino acid domain first identified in the $p40^{phox}$ and $p47^{phox}$ subunits of NADPH oxidase (*11*) and since found in many other proteins, e.g., the yeast t-SNARE Vam7p and the sorting nexin SNX3. In general, PX domains consist of three β-strands forming an antiparallel β-sheet, followed by three α-helices (Figure 1) (*12*). PX domains contain two highly conserved motifs: a RR(F/Y)(S)(D/E)F motif and a proline-rich motif (PP_{II}). The first motif is located in the β3−α1 region. Conserved basic residues (especially of the first motif) are implicated in interactions with PIs. Moreover, the proline-rich motif located between helix α1 and helix α2 (a conserved SH3-binding motif) and helix α2 itself correspond to the regions of the PX domains that are thought to interact with the membrane (*12*), via a membrane binding mechanism similar to that of FYVE (*1*, *13*, *14*). The loop region between the PP_{II} motif and helix α2 (i.e., located away from the binding pocket) is known as "membrane attachment loop" (*15*) and interacts with the interior as well as the surface of the membrane as it contains large, exposed hydrophobic residues. Moreover, it has been

[†]Research in M.S.P.S.'s laboratory is supported by the BBSRC, the EPSRC, and the Wellcome Trust. E.P. was supported by a Wellcome Trust Structural Biology studentship.

*To whom correspondence should be addressed. E-mail: mark.sansom@bioch.ox.ac.uk. Telephone: +44(0)1865 613306. Fax: +44 (0)1865 613238.

[1]Abbreviations: DPPC, dipalmitoylphosphatidylcholine; EEA1, early endosome antigen 1; $Ins(1,3)P_2$, inositol 1,3-bisphosphate; MD, molecular dynamics; PDB, Protein Data Bank; PI, phosphosinositide; PH, pleckstrin homology; PIP_2, phosphatidylinositol 4,5-bisphosphate; PME, particle mesh Ewald; PI(3)P, phosphatidylinositol 3-phosphate; PX, Phox homology (PX); rmsd, root-mean-square deviation; rmsf, root-mean-square fluctuation.

 Published on Web 05/01/2009

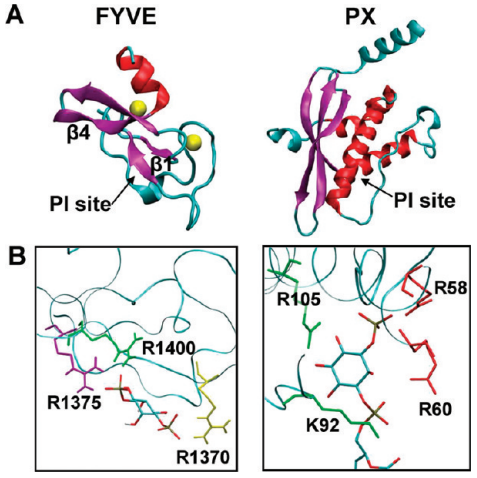

FIGURE 1: X-ray structures of the EAA1-FYVE (PDB entry 1JOC) and $p40^{phox}$-PX (PDB entry 1H6H) domains. (A) Cartoons of the protein domain folds with the PI-binding sites indicated. The two Zn ions are shown in the FYVE structure as yellow spheres. (B) Nature of the protein−Ins(1,3)P_2 (for FYVE) and protein−PI(3)P (for PX) interactions in the X-ray structures, with key basic side chains labeled.

suggested (*16*) that the $\beta1-\beta2$ loop may penetrate the membrane, as in most PX domains this loop contains hydrophobic and basic residues.

To improve our understanding of the mechanisms of the interactions of FYVE and PX domains with cell membranes, we can model their interactions with PI-containing lipid bilayers. Computer simulations of protein−bilayer interactions (*17*) provide a powerful tool for probing such dynamic interactions in atomistic detail, which has been shown, e.g., for a PH domain interacting with PIP_2 (*18*). In related approaches, e.g., continuum electrostatics calculations have been used to probe the membrane interactions of FYVE domains (*9*), and datum-driven docking has been used to explore interactions of FYVE and PX domains with detergent micelles (*19*). In this study, we use atomistic MD simulations to compare two PI(3)P-binding domains in terms of their interactions with a lipid bilayer. Thus, we compare simulations of the EEA1-FYVE domain and the $p40^{phox}$-PX domain and, in particular, focus on their interactions with PI(3)P-containing lipid bilayers. We address two key questions: (i) the location of these domains on the membrane and (ii) their interactions with the lipids, both specific interactions via bound PIs and nonspecific interactions with bilayer phospholipids.

EXPERIMENTAL PROCEDURES

Simulation Protocol. The GROMACS 3.0 simulation package (www.gromacs.org) (*20*, *21*) was used for all simulations, with a united atom GROMOS96 force field (*22*) and the SPC water model (*23*). Periodic boundary conditions were applied to the systems. Long-range electrostatics were calculated using the PME (particle mesh Ewald) method (*24*, *25*) with a real-space cutoff of 10 Å. For the van der Waals interactions, a cutoff of 10 Å was used. Simulations in water were performed at 300 K and in DPPC bilayers at 323 K, using a Berendsen thermostat (*26*) with a coupling constant (τ_T) of 0.1 ps. A constant pressure of 1 bar was maintained using a Berendsen barostat with an isotropic (for water simulations) or semi-isotropic (for bilayer simulations) coupling constant (τ_P) of 1.0 ps and a compressibility of 4.5×10^{-5} bar^{-1}. The integration time step was 2 fs for simulations in water and 1 fs for bilayer simulations. The LINCS method (*27*) was used to constrain bond lengths. Coordinates were saved every 5 ps for analysis. Analysis of all simulations was performed using the GROMACS package. VMD (*28*), PyMol (www.pymol.org), and RasTop [http://sourceforge.net/projects/rastop/ (*29*)] were used for visualization.

FYVE Structure. The X-ray structure of the FYVE domain from the early endosome autoantigen (EEA1; PDB entry 1JOC, 2.2 Å resolution) (*4*) was used as the starting structure for the simulations. In this structure, the FYVE domain forms a homodimer via interactions made by an extended coiled coil (from residues 1289−1347). In the simulations, just the monomeric, core domain (residues 1346−1411 of EEA1) was used. The X-ray structure has a molecule of Ins(1,3)P_2 [the headgroup of the lipid PI(3)P] bound to each monomer.

The FYVE domain contains a Zn finger, with two Zn ions each coordinated by four cysteines. The Hγ atom of each of these cysteine side chains was converted to a dummy atom. Terms were added for S−Zn bonds and Cβ−S−Zn bond angles for each Zn ion and their four ligating cysteine residues. The charge on each Zn ion was converted from +2 to +0.7, and the resultant negative charge was spread over each cysteine S atom (−0.175 each). Trial simulations indicated that this treatment maintained the stereochemistry of the Zn finger.

All ionizable residues were assigned their standard charge state at neutral pH, yielding a net charge of $+4e$. The net system charge was neutralized by addition of counterions. The protein structure was energy-minimized using 100 steps of steepest descents prior to simulation setup.

PX Structure. The X-ray structure of the PX domain from the $p40^{phox}$ subunit of NAPDH (PDB entry 1H6H, 1.7 Å resolution) (*30*) was used as the starting structure for the simulations. In this entry, the PX domain was bound to a phosphatidylinositol 3-phosphate [PI(3)P] molecule. All ionizable residues were assigned their standard charge state at neutral pH, yielding a net charge of $-2e$. The net system charge was neutralized by addition of counterions. The protein structure was energy-minimized using 100 steps of steepest descents prior to the simulation setup.

PI(3)P. GROMACS topologies for Ins(1,3)P_2 and PI(3)P were generated using PRODRG (*31*) (http://davapc1.bioch.dundee.ac.uk/programs/prodrg/). An Ins(1,3)P_2 model was energy-minimized and evaluated via a 10 ns simulation in water. A PI(3)P was constructed by joining Ins(1,3)P_2 to a dipalmitoylglycerol moiety. The PI(3)P model structure was energy-minimized and evaluated via a 1 ns simulation in water.

Simulation Systems. Three simulations were performed for each domain, as summarized in Table 1. Thus, six simulations were performed, for a total time of 0.1 μs. Procedures for the system setup are described in detail in ref (*18*). In the bilayer simulations, the initial orientation of the protein was such that the crystallographic Ins(1,3)P_2 molecule was superimposed on the headgroup of a PI(3)P molecule preinserted in a DPPC bilayer (see Figure 2). The resultant system was solvated and energy-minimized, followed by a short (0.2 ns) simulation run with position restraints on the non-H atoms of the protein (with a force constant of 1000 kJ mol^{-1} nm^{-1}) prior to the unrestrained production mode simulation.

RESULTS

Conformational Stability and Flexibility. The influence of PI(3)P binding on the conformational stability of both domains

Table 1: Summary of Simulations

simulation	system	atoms	time (ns)	Cα rmsd[a] (Å)
FYVE-Apo	FYVE and 4410 waters	13896	10	5.2
FYVE-IP2	FYVE, Ins(1,3)P_2, and 4402 waters	13893	10	2.5
FYVE-Bil	FYVE, PI(3)P, 240 DPPC, and 14068 waters	54934	30	2.5
PX-Apo	PX and 8316 waters	26424	10	4.4 (2.8)
PX-IP2	PX, Ins(1,3)P_2, and 8304 waters	26403	10	4.4 (2.8)
PX-Bil	PX, PI(3)P, 245 DPPC, and 18704 waters	69908	30	5.9 (2.7)

[a] The value given is the root-mean-square deviation (rmsd) for the Cα atoms of all residues, averaged over the final 2.5 ns of the 10 ns duration simulations, and over the final 5 ns of the 30 ns duration simulations. In each case, the reference frame is the X-ray structure. For the PX simulations, the value in parentheses is the Cα rmsd evaluated after exclusion of the first 20 residues at the N-terminus.

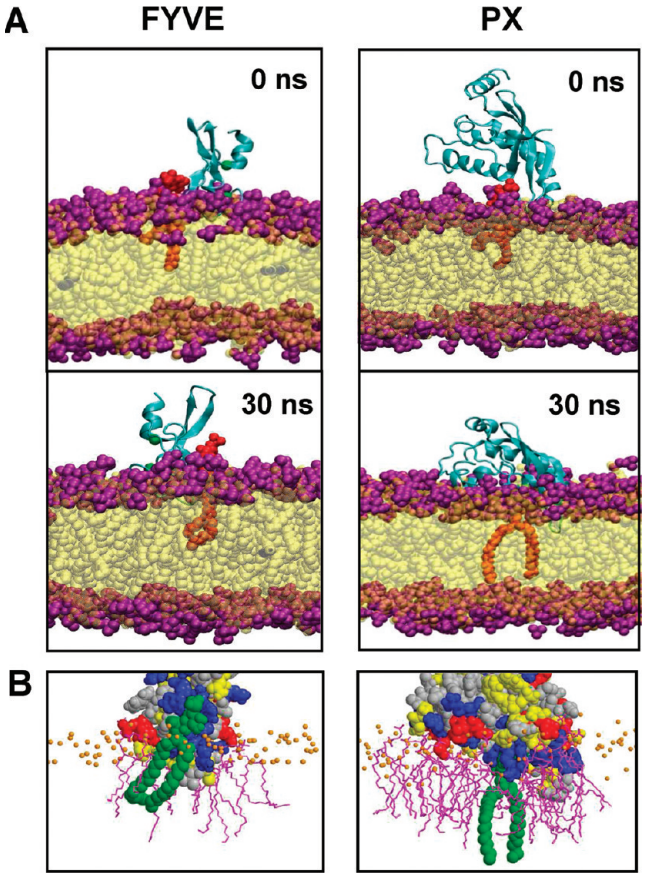

FIGURE 2: FYVE−bilayer and PX−bilayer interactions. (A) Snapshots are shown at the start (i.e., at 0 ns) and end (30 ns) of each bilayer simulation. Both proteins are in the cyan ribbon format; the lipid (DPPC) molecules are colored yellow with headgroups colored purple, and the PI(3)P is colored red/orange. (B) Detailed view of the interactions between the protein and those lipid molecules within a 3.5 Å cutoff distance of the protein, as seen in the 30 ns snapshots of each simulation. The protein atoms are colored blue (basic residues), red (acidic), yellow (polar), or gray (hydrophobic). The PI(3)P molecule is colored green. DPPC molecules forming contacts are shown in bonds format in purple. The small brown spheres represent the phosphorus atoms of lipid headgroups.

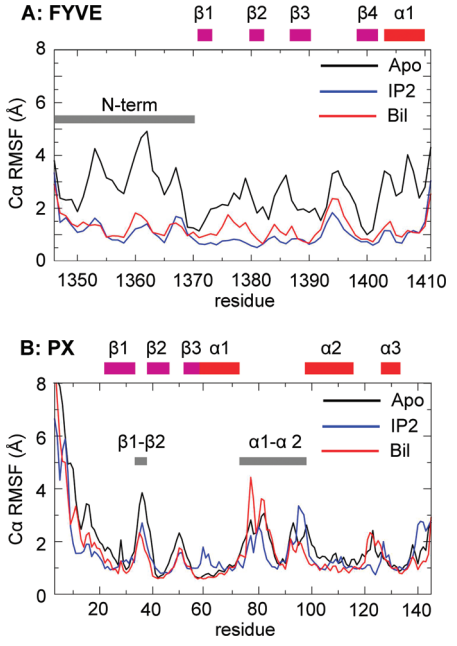

FIGURE 3: Root-mean-square fluctuations (rmsfs) of the Cα atoms as a function of residue number for the (A) FYVE and (B) PX simulations. In each case, rmsf profiles are shown for the apo (black), IP2 (blue), and Bil (red) simulations (see Table 1 for details). The locations of the secondary structure elements within each domain are indicated by the horizontal bars above the graphs.

was explored by calculating the conformational drift of the domains (as measured by the Cα rmsd) from their respective X-ray structures, both for simulations of the isolated domains in water bound to the PI(3)P headgroup [i.e., Ins(1,3)P_2] and for simulations of the domains bound to a single PI(3)P molecule in a DPPC bilayer (Table 1). For the FYVE domain, the Cα rmsd value is significantly lower in the PI(3)P−bilayer simulation (2.5 Å) than in the Ins(1,3)P_2−water simulation (5.2 Å), whereas for the PX domain, these two values (2.7 and 2.8 Å, respectively) were almost the same. More detailed examination of root-mean-square fluctuations (rmsfs) as a function of residue number (Figure 3) showed that for the FYVE domain, the regions interacting with both the PI(3)P ligand and the DPPC lipids exhibited enhanced flexibility in the water simulation.

From this analysis, it is evident that the FYVE domain exhibits significant internal mobility when in water, with the most flexible region being the N-terminal hydrophobic loop. This region (see below) interacts with the lipids in the bilayer simulation, reducing its flexibility. The presence of bound PI(3)P and to a lesser extent interactions with the bilayer also reduce significantly the flexibility of regions involved in PI binding. In contrast, the PX domain exhibited a similar degree of flexibility in both water and when bound to a bilayer, differing in this respect both from the FYVE domain and from the PH domain (*18*).

Bilayer Simulations. Visual inspection of the structures at the beginning and at the end of the FYVE-Bil and PX-Bil simulations (Figure 2) revealed that both domains remained bound to PI(3)P throughout the 30 ns duration simulations and interacted progressively as a function of time with the other

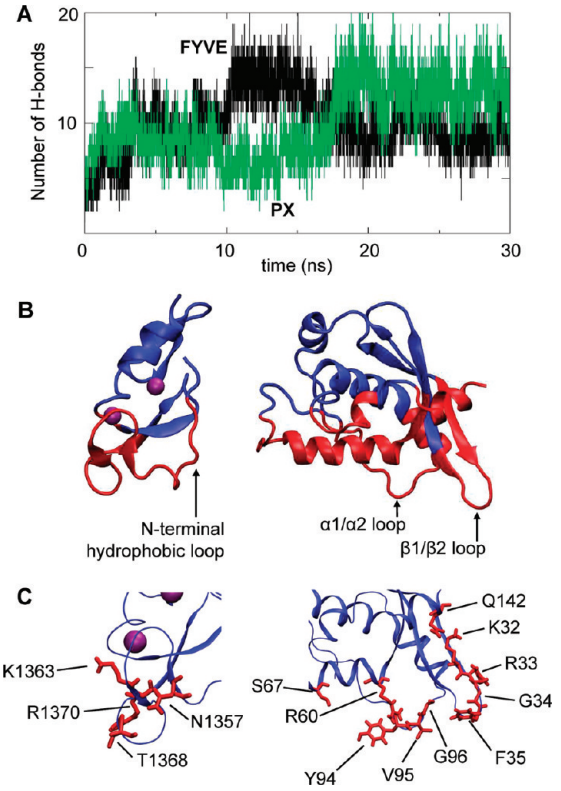

FIGURE 4: (A) Insertion of FYVE domains and PX into the bilayer. Number of hydrogen bonds between the FYVE domain and lipids (black line) or between the PX domain and lipids (green line), both as a function of time. (B) Regions of the FYVE and PX domains interacting with lipids. Residues of the FYVE and PX domains which interact with lipid molecules are colored red. The N-terminal hydrophobic loop of the FYVE domain and the $\beta1-\beta2$ and $\alpha1-\alpha2$ loops of the PX domain which form nonspecific contacts with the bilayer are indicated. For each snapshot, the structure of the protein at the end (30 ns) of the bilayer simulations is shown. (C) Residues (red) of the FYVE and PX domains forming ~70% of the H-bonds with bilayer lipids over the course of each simulation.

(DPPC) lipid molecules of the bilayer. Comparison of the snapshots suggested that the headgroup of the PI(3)P molecule in the PX domain simulation inserted more deeply into the bilayer. This was confirmed by measuring the distance between the center of mass of the PI(3)P headgroup and the center of mass of the DPPC bilayer along the *z*-axis. This distance decreased from ~27 Å at 0 ns in each bilayer simulations to ~15 Å in the PX simulation, but to only ~25 Å in the FYVE domain simulation over the course of 30 ns. Moreover, from these snapshots, it is evident that in both cases the protein also inserted further into the bilayer. This was confirmed by the decrease in the distance between the center of mass of the domains and of the bilayer along the bilayer normal. During both 30 ns bilayer simulations, this distance decreased from ~43 Å for the PX domain and ~33 Å for the FYVE domain to ~28 Å for both domains.

Protein−Lipid Interactions. In both cases, visualization of insertion of the domains into the bilayer suggests the formation of (nonspecific) protein−lipid contacts. Analysis of the total number of protein−lipid H-bonds (Figure 4A) reveals this to increase from ~2 at 0 ns to ~8 at 30 ns for FYVE, and from ~0 to ~13 for PX.

To also identify potential hydrophobic interactions, we analyzed protein residues that were close (6 Å cutoff) to the lipids (all atoms) over the final 5 ns of both bilayer simulations (Figure 4B). For the EEA1-FYVE domain, there was one main region interacting with the lipids. This corresponded to residues W1349−H1372, i.e., residues of the hydrophobic N-terminal loop with additional residues A1383 and E1384 (Figure 4B). This is in good agreement with experimental studies (*3*, *4*, *7*, *8*) that suggested penetration of this loop into the membrane. More detailed analysis showed that four residues (N1357, K1363, T1368, and R1370) of this loop formed ~75% of the H-bonds of the FYVE domain with the bilayer.

For the p40^{phox}-PX domain, similar analysis showed that the main contacts with the bilayer were the $\beta1-\beta2$ loop, the $\alpha1-\alpha2$ loop, and helix $\alpha2$. Less extensive contacts were formed by the $\beta3-\alpha1$ loop, helix $\alpha1$, and the 10 C-terminal residues of the domain (Figure 4B). Just 10 residues (K32, R33, G34, and F35 in the $\beta1-\beta2$ loop, R60 and S67 in the $\alpha1$ helix, Y94, V95, and G96 in the $\alpha1-\alpha2$ loop, and Q142 at the C-terminus) formed ~65% of the hydrogen bonds of the PX domain with the lipids. Just four residues of the $\beta1-\beta2$ loop and two residues of the $\alpha1-\alpha2$ loop interacted with both the polar and the nonpolar atoms of the lipids. These results agree with experiments which had identified the $\alpha1-\alpha2$ loop [the membrane attachment loop (*15*)] and helix $\alpha2$ as the main bilayer contacts (*12*, *14*, *32*−*34*). It has also been suggested (*16*) that the $\beta1-\beta2$ loop penetrates the membrane. Again, this is in agreement with the analysis given above, which also suggests an additional region, the C-terminus, interacts significantly with the headgroups of the lipids.

Previous studies of the EAA1-FYVE domain (*5*, *19*) have implicated V1367, T1368, and R1370 in interactions with bilayer lipids. If we exclude the interactions of these residues (see Figure 4C) from our analysis of H-bonding interactions within the protein−bilayer complex, more than 50% of H-bonding interactions are lost. Similarly, for the p40^{phox}-PX domain, it has been reported that F35, Y94, and V95 are involved in membrane interactions (*14*). These residues (see Figure 4C) form four of the 13 persistent H-bonds between lipids and the protein in our simulations. Furthermore, it has been reported (*14*) that the L82A mutation does not alter the penetration of the bilayer by the PX domain. This also is in agreement with the MD simulations, as this residue was not found to interact with the lipids.

Protein−PI(3)P Interactions. It was also important to characterize in detail the interactions of the FYVE and PX domains with PI(3)P while in a membrane (i.e., lipid bilayer) environment. Analysis of the residues of the EEA1-FYVE domain forming the closest contacts to the phosphates, P1 and P3, of PI(3)P at positions 1 and 3 of the inositol ring (cutoff of 6 Å) revealed that the closest residues were R1371, H1372, H1373, R1375, I1380, K1397, and R1400. Further analysis (Figure 5A) of these contacts showed that P1 formed weaker interactions with R1371, H1372, H1373, and R1375. The most pronounced interaction of P1 was with R1371 until ~28 ns, when this interaction weakened and was replaced by those with which the other three residues interacted. P3 interacted with H1372, H1373, R1375, and R1400 during the 30 ns simulation, but all these interactions fluctuated. This confirms what was found experimentally (*4*), i.e., that P3 interacts with the small charged pocket formed by the residues listed above. Finally, the residues forming the closest contacts to the PI(3)P tails were D1352, N1353, Q1356, F1365, S1366, V1367, R1370, and R1371.

A comparable analysis for the PX domain revealed the closest residues to P1 and P3 to be F39, R58, Y59, R60, H63, K92, K98, and R105. Specifically, P1 initially interacted with R60 and H63 (Figure 5B). At ~2 ns, the R60−P1 interaction weakened, and while the interaction of K92 with P1 strengthened, at 5 ns the

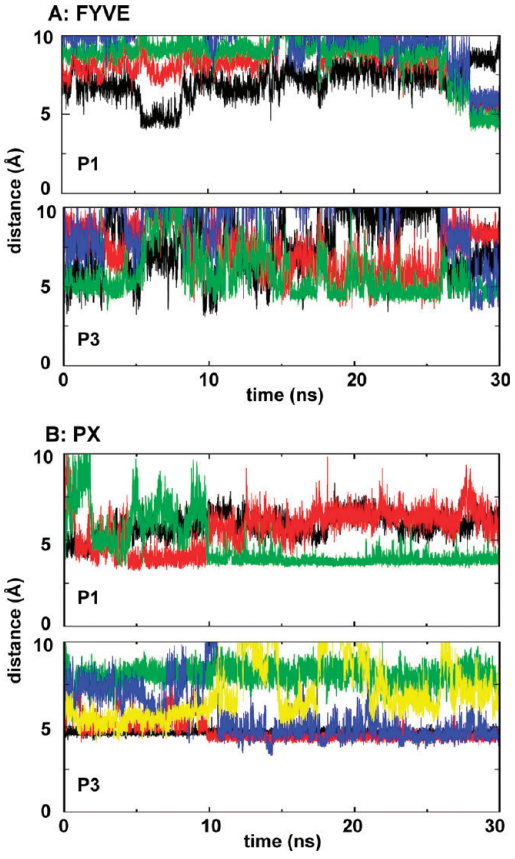

FIGURE 5: Residue−phosphate distances for the FYVE and PX domain bilayer simulations. (A) Distances between the phosphorus atom and the CZ (for arginines) or ND1/NE1 (for histidine) atoms of interacting basic residues for the FYVE domain bilayer simulation. Distances are shown for P1 with R1371 (black), H1372 (red), H1373 (green), and R1375 (blue) and for P3 with H1372 (black), H1373 (red), R1375 (green), and R1400 (blue). (B) Distances between the phosphorus atom and the NZ (for lysines), CZ (for arginines), or ND1/NE1 (for histidine) atoms of interacting basic residues for the PX domain bilayer simulation. Distances are shown for P1 with R60 (black), H63 (red), and K92 (green) and for P3 with R58 (black), R60 (red), H63 (green), K98 (blue), and R105 (yellow).

latter interactions weakened as well. At ~10 ns, a switch occurred such that the H63−P1 interaction weakened and was replaced by the K92−P1 interaction. After ~10 ns, P1 formed a tight interaction with K92 and weaker interactions with R60 and H63. P3 interacted with R58 and R60 throughout the simulation. Initially, P3 formed tight interactions with R105 and a weaker interaction with K98. At ~10 ns, the R105−/P3 interaction weakened, being replaced by the K98−P3 interaction. Until the end of the simulation, the interaction of P3 with R105 fluctuated but with K98 remained stable and tight. R105 was in the proximity of 4- and 5-hydroxyl groups of the inositol headgroup, in agreement with experimental data (*30*). Finally, there were three residues that formed the closest contacts to the PI(3)P tails: R60, K92, and Y94. Y94, located in the membrane attachment loop, interacted in the crystal structure (*30*) with the carbons of the glycerol moiety of PI(3)P.

DISCUSSION

It is of interest that the PX and FYVE domains behaved differently in the PI(3)P and in the bilayer simulations. The FYVE domain appeared to interact more weakly with the ligand (i.e., with more transient phosphate−side chain interactions) than did the PX domain. In the FYVE domain bilayer simulation, P3 interacted with both R1400 and the charged pocket created by the HHCR motif. There has been some discussion of the role of R1400 in P3 binding. Thus, in the X-ray structure (*4*), R1400 is not oriented appropriately for a direct H-bond to P3. In the NMR datum-driven docking calculations for the micelle complex (*19*), R1400 is suggested to H-bond to P3. It is therefore of interest that the MD simulations also point to the existence of such an interaction. In contrast to the FYVE domain, for the PX domain P3 interacted more strongly with the protein than did P1. Again, the residues of the PX domain interacting with P1 and P3 were in agreement with experimental studies.

In terms of nonspecific interactions with lipids, only one region of the FYVE domain interacted with the lipids, namely the N-terminal hydrophobic loop. The degree of insertion of the FYVE domain into the bilayer was smaller than that of the PX domain, and with the FYVE domain, the headgroup of PI(3)P did not become buried deeper within the bilayer. It should be noted that in control simulations (data not shown) of PI(3)P in a DPPC bilayer in the absence of protein, the headgroup of the phosphoinositide did not insert into the bilayer (over 10 ns). This suggests that insertion of the headgroup of PI(3)P into the bilayer in the presence of the PX domain was due to the presence of the protein. The smaller degree of insertion, and hence greater exposure of the headgroup to water in the presence of FYVE, may explain the more transient nature of the phosphate−basic side chain interactions for this domain relative to the PX domain.

In summary, the results of these simulations for the interactions of the domains with lipids and the phosphoinositides are in broad agreement with the available experimental data (*3*, *35*, *36*). However, they clearly reveal additional regions which interact with bilayer lipids that are not seen either in experiments (mainly performed in a micellar environment) or in simulations with PI(3)P-containing detergent micelles (data not shown). Hence, the MD simulations have revealed additional regions of interactions and the equilibrium position of the PI(3)P-bound domains when in a zwitterionic lipid bilayer.

In the simulation protocol adopted in this study, the protein is positioned at the surface of the bilayer at the start of the simulation, thus assuming an approximate orientation of the protein relative to the bilayer. Both coarse-grained (*18*) and atomistic (Lumb, Stansfeld, and M. S. P. Sansom, unpublished data) simulations of PH domains initially positioned distant from (and randomly oriented relative to) a bilayer suggest that the initial protein−bilayer contact can also be simulated. However, a multiscale simulation approach (*37*, *38*) may be required to enable the complete process of bilayer encounter followed by phosphoinositide binding to be simulated. A multiscale method has recently been used to explore interactions of the lipid bilayer with BAR domains (*39*). In this context, development of such multiscale simulations may also enable exploration of possible bilayer curvature effects of the EEA1-FYVE domain dimer (a monomeric construct used in this study).

Despite these limitations, the computational approach used in this study is quite general. The good agreement with experiment suggests it may be applicable when biophysical data are not available to predict membrane interaction mechanisms of PI-recognizing and related domains. The method can be extended to accommodate interactions with, e.g., anionic lipids within the bilayer (*3*) and to multidomain proteins. In this way, simulation approaches to PI-binding domains and to other

membrane-binding domains [e.g., C2 (*40*)] may be combined to reconstruct the nature of dynamic complexes at the cell membrane surface.

REFERENCES

1. Cho, W., and Stahelin, R. V. (2005) Membrane-protein interactions in cell signaling and membrane trafficking. *Annu. Rev. Biophys. Biomol. Struct.*34, 119–151.
2. Wakelam, M. J. O. (2007) in Biochemical Society Symposia, pp 277, Portland Press, London.
3. Kutateladze, T. G. (2007) Mechanistic similarities in docking of the FYVE and PX domains to phosphatidylinositol 3-phosphate containing membranes. *Prog. Lipid Res.*46, 315–327.
4. Dumas, J. J., Merithew, E., Sudharshan, E., Rajamani, D., Hayes, S., Lawe, D., Corvera, S., and Lambright, D. G. (2001) Multivalent endosome targeting by homodimeric EEA1. *Mol. Cell*8, 947–958.
5. Kutateladze, T., and Overduin, M. (2001) Structural mechanism of endosome docking by the FYVE domain. *Science*291, 1793–1796.
6. Misra, S., and Hurley, J. H. (1999) Crystal structure of a phosphatidylinositol 3-phosphate-specific membrane-targeting motif, the FYVE domain of Vps27p. *Cell*97, 657–666.
7. Kutateladze, T. G., Capelluto, D. G., Ferguson, C. G., Cheever, M. L., Kutateladze, A. G., Prestwich, G. D., and Overduin, M. (2004) Multivalent mechanism of membrane insertion by the FYVE domain. *J. Biol. Chem.*279, 3050–3057.
8. Stahelin, R. V., Long, F., Diraviyam, K., Bruzik, K. S., Murray, D., and Cho, W. (2002) Phosphatidylinositol 3-phosphate induces the membrane penetration of the FYVE domains of Vps27p and Hrs. *J. Biol. Chem.*277, 26379–26388.
9. Diraviyam, K., Stahelin, R. V., Cho, W., and Murray, D. (2003) Computer modeling of the membrane interaction of FYVE domains. *J. Mol. Biol.*328, 721–736.
10. Callaghan, J., Simonsen, A., Gaullier, J. M., Toh, B. H., and Stenmark, H. (1999) The endosome fusion regulator early-endosomal autoantigen 1 (EEA1) is a dimer. *Biochem. J.*338, 539–543.
11. Ponting, C. P. (1996) Novel domains in NADPH oxidase subunits, sorting nexins, and PtdIns 3-kinases: Binding partners of SH3 domains?. *Protein Sci.*5, 2353–2357.
12. Xu, Y., Seet, L. F., Hanson, B., and Hong, W. (2001) The Phox homology (PX) domain, a new player in phosphoinositide signalling. *Biochem. J.*360, 513–530.
13. Karathanassis, D., Stahelin, R. V., Bravo, J., Perisic, O., Pacold, C. M., Cho, W., and Williams, R. L. (2002) Binding of the PX domain of p47(phox) to phosphatidylinositol 3,4-bisphosphate and phosphatidic acid is masked by an intramolecular interaction. *EMBO J.*21, 5057–5068.
14. Stahelin, R. V., Burian, A., Bruzik, K. S., Murray, D., and Cho, W. (2003) Membrane binding mechanisms of the PX domains of NADPH oxidase p40phox and p47phox. *J. Biol. Chem.*278, 14469–14479.
15. Wishart, M. J., Taylor, G. S., and Dixon, J. E. (2001) Phoxy lipids: Revealing PX domains as phosphoinositide binding modules. *Cell*105, 817–820.
16. Misra, S., Miller, G. J., and Hurley, J. H. (2001) Recognizing phosphatidylinositol 3-phosphate. *Cell*107, 559–562.
17. Lindahl, E., and Sansom, M. S. P. (2008) Membrane proteins: Molecular dynamics simulations. *Curr. Opin. Struct. Biol.*18, 425–431.
18. Psachoulia, E., and Sansom, M. S. P. (2008) Interactions of the pleckstrin homology domain with phosphatidylinositol phosphate and membranes: Characterization via molecular dynamics simulations. *Biochemistry*47, 4211–4220.
19. Dancea, F., Kami, K., and Overduin, M. (2008) Lipid interaction networks of peripheral membrane proteins revealed by data-driven micelle docking. *Biophys. J.*94, 515–524.
20. Lindahl, E., Hess, B., and van der Spoel, D. (2001) GROMACS 3.0: A package for molecular simulation and trajectory analysis. *J. Mol. Model.*7, 306–317.
21. van der Spoel, D., Lindahl, E., Hess, B., Groenhof, G., Mark, A. E., and Berendsen, H. J. (2005) GROMACS: Fast, flexible, and free. *J. Comput. Chem.*26, 1701–1718.
22. van Gunsteren, W. F., Kruger, P., Billeter, S. R., Mark, A. E., Eising, A. A., Scott, W. R. P., Huneberger, P. H., and Tironi, I. G. (1996) Biomolecular Simulation: The GROMOS96 Manual and User Guide, Biomos & Hochschulverlag AG an der ETH Zurich, Groningen, The Netherlands.
23. Hermans, J., Berendsen, H. J. C., van Gunsteren, W. F., and Postma, J. P. M. (1984) A consistent empirical potential for water-protein interactions. *Biopolymers*23, 1513–1518.
24. Darden, T., York, D., and Pedersen, L. (1993) Particle mesh Ewald: An N.log(N) method for Ewald sums in large systems. *J. Chem. Phys.*98, 10089–10092.
25. Essmann, U., Perera, L., Berkowitz, M. L., Darden, T., Lee, H., and Pedersen, L. G. (1995) A smooth particle mesh Ewald method. *J. Chem. Phys.*103, 8577–8593.
26. Berendsen, H. J. C., Postma, J. P. M., van Gunsteren, W. F., DiNola, A., and Haak, J. R. (1984) Molecular dynamics with coupling to an external bath. *J. Chem. Phys.*81, 3684–3690.
27. Hess, B., Bekker, H., Berendsen, H. J. C., and Fraaije, J. G. E. M. (1997) LINCS: A linear constraint solver for molecular simulations. *J. Comput. Chem.*18, 1463–1472.
28. Humphrey, W., Dalke, A., and Schulten, K. (1996) VMD: Visual Molecular Dynamics. *J. Mol. Graphics*14, 33–38.
29. Sayle, R. A., and Milner-White, E. J. (1995) RasMol: Biomolecular graphics for all. *Trends Biochem. Sci.*20, 374–376.
30. Bravo, J., Karathanassis, D., Pacold, C. M., Pacold, M. E., Ellson, C. D., Anderson, K. E., Butler, P. J., Lavenir, I., Perisic, O., Hawkins, P. T., Stephens, L., and Williams, R. L. (2001) The crystal structure of the PX domain from p40(phox) bound to phosphatidylinositol 3-phosphate. *Mol. Cell*8, 829–839.
31. van Aalten, D. M., Bywater, R., Findlay, J. B., Hendlich, M., Hooft, R. W., and Vriend, G. (1996) PRODRG, a program for generating molecular topologies and unique molecular descriptors from coordinates of small molecules. *J. Comput.-Aided Mol. Des.*10, 255–262.
32. Kanai, F., Liu, H., Field, S. J., Akbary, H., Matsuo, T., Brown, G. E., Cantley, L. C., and Yaffe, M. B. (2001) The PX domains of p47phox and p40phox bind to lipid products of phosphoinositide 3-kinase. *Nat. Cell Biol.*3, 675–678.
33. Cheever, M. L., Sato, T. K., de Beer, T., Kutateladze, T. G., Emr, S. D., and Overduin, M. (2001) Phox domain interaction with Ptdlns(S) P targets the Vam7 t-SNARE to vacuole membranes. *Nat. Cell Biol.*3, 613–618.
34. Sato, T. K., Overduin, M., and Emr, S. D. (2001) Location, location, location: Membrane targeting directed by PX domains. *Science*294, 1881–1885.
35. Brunecky, R., Lee, S., Rzepecki, P. W., Overduin, M., Prestwich, G. D., Kutateladze, A. G., and Kutateladze, T. G. (2005) Investigation of the binding geometry of a peripheral membrane protein. *Biochemistry*44, 16064–16071.
36. Malkova, S., Stahelin, R. V., Pingali, S. V., Cho, W., and Schlossman, M. L. (2006) Orientation and penetration depth of monolayer-bound $p40^{phox}$-PX. *Biochemistry*45, 13566–13575.
37. Sherwood, P., Brooks, B. R., and Sansom, M. S. P. (2008) Multiscale methods for macromolecular simulations. *Curr. Opin. Struct. Biol.*18, 630–640.
38. Ayton, G. S., Izvekov, S., Noid, W. G., and Voth, G. A. (2008) Multiscale simulation of membranes and membrane proteins: Connecting molecular interactions to mesoscopic behavior. *Curr. Top. Membr.*60, 181–225.
39. Arkhipov, A., Yin, Y., and Schulten, K. (2008) Four-scale description of membrane sculpting by BAR domains. *Biophys. J.*95, 2806–2821.
40. Jaud, S., Tobias, D. J., Falke, J. J., and White, S. H. (2007) Self-induced docking site of a deeply embedded peripheral membrane protein. *Biophys. J.*92, 517–524.